agronomy

MDPI

Article

Coupling Remote Sensing Data and AquaCrop Model for Simulation of Winter Wheat Growth under Rainfed and Irrigated Conditions in a Mediterranean Environment

Marie Therese Abi Saab [1,*], Razane El Alam [2], Ihab Jomaa [3], Sleiman Skaf [3], Salim Fahed [1], Rossella Albrizio [4,*] and Mladen Todorovic [2]

1 Lebanese Agricultural Research Institute, Fanar P.O. Box 90-1965, Lebanon; salimfahed@gmail.com
2 CIHEAM—Mediterranean Agronomic Institute of Bari, Via Ceglie 9, 70010 Valenzano, BA, Italy; razane.elalam@gmail.com (R.E.A.); mladen@iamb.it (M.T.)
3 Lebanese Agricultural Research Institute, Tal Amara P.O. Box 287, Lebanon; ijomaa@lari.gov.lb (I.J.); sleimskaf@hotmail.com (S.S.)
4 National Research Council of Italy, Institute for Agricultural and Forestry Systems in the Mediterranean (CNR–ISAFOM), P. le E. Fermi, 1, Porto del Granatello, 80055 Portici, NA, Italy
* Correspondence: mtabisaab@lari.gov.lb (M.T.A.S.); rossella.albrizio@cnr.it (R.A.)

Abstract: The coupling of remote sensing technology and crop growth models represents a promising approach to support crop yield prediction and irrigation management. In this study, five vegetation indices were derived from the Copernicus-Sentinel 2 satellite to investigate their performance monitoring winter wheat growth in a Mediterranean environment in Lebanon's Bekaa Valley. Among those indices, the fraction of canopy cover was integrated into the AquaCrop model to simulate biomass and yield of wheat grown under rainfed conditions and fully irrigated regimes. The experiment was conducted during three consecutive growing seasons (from 2017 to 2019), characterized by different precipitation patterns. The AquaCrop model was calibrated and validated for different water regimes, and its performance was tested when coupled with remote sensing canopy cover. The results showed a good fit between measured canopy cover and Leaf Area Index (LAI) data and those derived from Sentinel 2 images. The R^2 coefficient was 0.79 for canopy cover and 0.77 for LAI. Moreover, the regressions were fitted to relate biomass with Sentinel 2 vegetation indices. In descending order of R^2, the indices were ranked: Fractional Vegetation Cover (FVC), LAI, the fraction of Absorbed Photosynthetically Active Radiation (fAPAR), the Normalized Difference Vegetation Index (NDVI), and the Enhanced Vegetation Index (EVI). Notably, FVC and LAI were highly correlated with biomass. The results of the AquaCrop calibration showed that the modeling efficiency values, NSE, were 0.99 for well-watered treatments and 0.95 for rainfed conditions, confirming the goodness of fit between measured and simulated values. The validation results confirmed that the simulated yield varied from 2.59 to 5.36 t ha^{-1}, while the measured yield varied from 3.08 to 5.63 t ha^{-1} for full irrigation and rainfed treatments. After integrating the canopy cover into AquaCrop, the % of deviation of simulated and measured variables was reduced. The Root Mean Square Error (RMSE) for yield ranged between 0.08 and 0.69 t ha^{-1} before coupling and between 0.04 and 0.42 t ha^{-1} after integration. This result confirmed that the presented integration framework represents a promising method to improve the prediction of wheat crop growth in Mediterranean areas. Further studies are needed before being applied on a larger scale.

Keywords: crop models; winter wheat; irrigation; Sentinel 2; vegetation indices; canopy cover

Citation: Abi Saab, M.T.; El Alam, R.; Jomaa, I.; Skaf, S.; Fahed, S.; Albrizio, R.; Todorovic, M. Coupling Remote Sensing Data and AquaCrop Model for Simulation of Winter Wheat Growth under Rainfed and Irrigated Conditions in a Mediterranean Environment. *Agronomy* **2021**, *11*, 2265. https://doi.org/10.3390/agronomy11112265

Academic Editor: Belen Gallego-Elvira

Received: 30 September 2021
Accepted: 7 November 2021
Published: 9 November 2021

1. Introduction

Current agri-food systems rely on relatively few staple crops; among them, cereal production is crucial for the Mediterranean region. However, impacts of climate change, water scarcity, growing population demand, and economic oscillations pose significant

challenges for agriculture and cereal production, particularly in semi-arid regions [1,2]. Among cereal crops, wheat is the most widely produced [3], constituting the stable crop for about half of the world's population [4], with a global annual production of about 730 million tons [5,6].

In Lebanon, wheat makes up almost 66% of the cultivated cereal crops. The Bekaa valley represents the food basket of the country, accounting for 58% of wheat production [7]. Nowadays, cereal yield fluctuates mainly due to scarce and erratic precipitation, high temperature variations, and a non-rational use of supplemental irrigation. The increasing water deficiency in the valley is the main factor threatening farmers to manage better water use for food production [8,9]. Indeed, a joint application of different technologies as crop growth models and remote sensing data may contribute to the achievements of this scope [10].

Crop growth models have been advancing in their applications during the last decades due to the increased availability of data necessary for simulation of crop development and growth as well as prediction of crop yields. Moreover, data acquisition technologies and remote sensing have been developing almost exponentially, providing a large volume of high-quality real-time data about the state of vegetation on the ground. Therefore, dynamic crop growth monitoring has begun to be effectively used in practice for the day-by-day evaluation of crop growth, taking into account different environmental factors and management decisions [11]. For this purpose, to improve the estimations, the insertion of valuable information from remote sensing measurements into crop model simulation processes is of particular importance.

Multiple kinds of variables such as the leaf area index (LAI) [12], soil moisture [13], normalized difference vegetation index (NDVI) [14], and fractional cover (FVC) [15] can be used for the integration of remote sensing data in crop growth models. The studies, with different degrees of success, have demonstrated the positive effects of these integration strategies on different crops [16–20]. Among the crops that were studied for yield forecasting, wheat was investigated by [21] through the integration of LAI in the EPIC model and by [22] through the assimilation of fc in AquaCrop. Maize crop was studied by [11,23,24], who assimilated both fc and biomass into the AquaCrop model. Ref. [15] reported a case study in Italy on the tomato crop with FVC assimilation in AquaCrop. However, the application of remote sensing to support prediction of crop growth and yield is still limited to developed countries, and it is poorly adopted in most countries of the Middle East and North Africa. Accordingly, the use of remote sensing and modelling tools might be particularly relevant for the southern Mediterranean countries. Therefore, it is of great interest to test the integration of remote sensing and modelling data in the Mediterranean areas where the efficient use of water and improvement of crop water productivity are among the priorities in stabilizing the yield (especially of cereals) and achieving food security.

The objectives of this study were (i) to investigate the performance of five vegetation indices derived from satellite data in respect to their correlation to field measurements; (ii) to calibrate and validate AquaCrop for assessing the response of winter wheat to different water management strategies; (iii) to examine the suitability of coupling the earth observation data with field observations and AquaCrop model for monitoring of winter wheat crop growth. Hence, the benefits of coupling remote-sensing data and a crop growth model to estimate the responses of winter wheat to different irrigation management options in a semi-arid Mediterranean area are assessed.

2. Materials and Methods

In this study, the data used was derived from field trials carried out at the experimental field of Lebanese Agricultural Research Institute (LARI) (33°51′44″ N latitude, 35°59′32″ E longitude and 905 m above sea level), in the Bekaa Valley of Lebanon, during three consecutive growing seasons (2016–2017, 2017–2018, 2018–2019). The location of the study area and the field trials are provided in Figure S1. Durum wheat (cv. Icarasha) was grown

under irrigated and rainfed conditions. The collected field data and measurements served for: (i) comparison of some variables estimated from the earth observations based on ESA-Sentinel-2 images and on-field ground measurements (datasets 2016–2017 and 2018–2019); (ii) calibration of the AquaCrop model under different water regimes (dataset of 2016–2017); (iii) validation of the AquaCrop model (datasets of 2017–2018 and 2018–2019); (iv) insertion of remote sensing variable (FVC) into AquaCrop (datasets 2016–2017 and 2018–2019).

2.1. Study Area and Field Trials

The Bekaa valley is an important agricultural plain where winter cereals and spring/summer vegetables are cultivated. Erratic rainfall, drought, and spring frost are the main challenges for cereal growers in the region [9]. The area is characterized by a Mediterranean climate with an average annual rainfall of 592 mm, mainly during autumn and winter months (October to March), while the summer season is hot and dry. Air temperature, relative humidity, solar radiation, wind speed, and rainfall were recorded from an experimental field's agro-meteorological station. Monthly weather data, from November 2016 to June 2019, are given in Table 1 together with the reference evapotranspiration (ETo) estimated by the FAO Penman–Monteith standard approach [25].

Table 1. Monthly climatic data as recorded from November 2016 until June 2019.

Month	Rain [mm Month^{-1}]	Tmax [°C]	Tmin [°C]	RHmean [%]	WS [m s^{-1}]	Rs [W m^{-21}]	ETo [mm Month^{-1}]
November-16	29.00	20.35	2.81	45.65	1.41	89.12	59.40
December-16	105.20	10.29	0.43	83.68	1.91	61.77	26.50
17 January	119.40	10.87	−0.73	78.87	1.69	68.20	30.70
17 February	14.20	13.70	−2.12	60.54	1.38	82.75	43.00
17 March	49.40	16.15	4.01	72.03	1.98	118.38	62.00
17 April	12.60	22.33	5.94	53.87	2.11	261.81	126.40
17 May	3.80	27.30	9.02	47.35	2.04	320.03	175.30
17 June	2.40	32.25	12.04	41.97	1.80	346.29	197.40
17 July	0.00	34.92	17.46	36.64	1.18	351.36	198.10
17 August	0.00	35.25	13.20	43.79	1.34	305.01	182.80
17 September	0.20	33.32	12.73	45.17	1.29	250.94	142.60
17 October	13.80	25.43	8.74	54.80	1.18	174.53	85.90
17 November	22.80	19.42	5.02	67.04	1.15	119.52	48.3
17 December	0.20	16.78	2.28	68.03	1.28	96.30	39.7
18 January	168.20	11.88	1.13	82.68	1.50	84.84	29.40
18 February	131.80	16.32	3.26	70.45	1.35	123.62	45.80
18 March	18.20	20.96	3.95	57.61	1.66	206.32	93.20
18 April	17.60	24.35	6.74	52.57	1.37	248.99	117.10
18 May	19.80	27.05	12.48	50.98	1.30	279.58	147.00
18 June	12.20	30.73	14.67	46.51	1.78	322.78	183.30
18 July	0.00	33.40	14.02	45.74	1.93	324.94	203.90
18 August	0.00	33.80	14.25	50.05	1.64	291.17	179.40
18 September	0.00	32.50	13.61	46.94	1.36	232.73	136.60
18 October	70.80	26.43	10.77	60.09	1.26	165.64	86.80
18 November	46.20	17.88	6.28	78.19	1.17	106.52	40.50
18 December	122.20	12.05	4.06	88.77	1.50	76.20	24.30
19 January	288.00	10.70	−0.15	83.45	1.73	102.05	29.80
19 February	214.40	12.69	1.34	81.97	1.45	126.49	37.10
19 March	130.00	14.78	3.09	75.97	1.70	172.19	64.40
19 April	75.60	18.38	4.71	72.63	1.31	222.68	86.90
19 May	13.80	29.62	9.35	45.12	1.19	320.70	163.60
19 June	4.00	32.63	13.81	49.31	1.46	332.87	183.00

The first two experimental seasons (2016–2017 and 2017–2018) were dry, with a precipitation amount in November–June of 336 and 390.8 mm, respectively. On the contrary, in the last experimental year (2018–2019), the precipitation was more than two times more significant, reaching for the same period (November–June) a total amount of 894.2 mm. When considering the period February–April, corresponding to short vegetation development and flowering, the precipitation was 76.2 mm in 2016–2017, 167.6 mm in 2017–2018, and 420 mm in 2018–2019.

For each season, soil samples were taken from the experimental field at up to 90 cm depth. Soils were described according to the guidelines for soil description [26] and classified according to [27]. In the three experimental seasons, soil hydrological properties were estimated from the soil granulometric analysis, the electrical conductivity, and the organic matter by using a pedo-transfer function as suggested by [28]. The results are presented in Table S1. The experiments were conducted in the same experimental farm but in three different fields in three years. Therefore, in the first year, the soil water holding capacity was 180 mm m^{-1}, while in the second it was almost 25% lower (136 mm m^{-1}), and 130 mm m^{-1} in the third season.

In the three growing seasons, durum wheat was sown in rows 0.18 m apart by utilizing 200 Kg of seeds per hectare. Nitrogen supply was 60 kg ha^{-1}; in particular, ammonium sulfate (21% N) and ammonium nitrate (26–27% N) were applied at the beginning of tillering and at the beginning of stem elongation, respectively.

In this study, the data of I-100% (full irrigation) and I-rainfed treatments were used. For the growing seasons 2016–2017 and 2017–2018, the data was derived from the trials described in [8]. The irrigation experiment consisted of nine plots, each 300 m^2 in size (15 m × 20 m). Irrigation was monitored using a smartphone application called Bluleaf [8]. From the booting until the grain-filling stages, irrigation was supplied back to field capacity each time that the soil water content dropped below the readily available water in the root zone, considered to be 55% of the total available water. Irrigated plots were equipped with traditional impact sprinklers (with a discharge rate of 1.5 m^3/h) overlaid on the middle of each plot. Each treatment had its valve and flow meter.

For the season 2018–2019, the trial consisted of a randomized complete block design, having three irrigation treatments and three replicates per treatment: I-100%, I-50% deficit irrigation, and I-rainfed. The size of each plot was 100 m^2 (10 m × 10 m), having the same disposition and orientation of the Sentinel 2A pixels.

In season 2016–2017, the total net irrigation amount for I-100 was 203 mm while in season 2017–2018, it was 248 mm. For the season 2018–2019, the total net irrigation amount was 72.6 mm for the I-100 treatment and 36.3 mm for I-50.

2.2. Field Observations and Measurements

For the three years of field trials, the crop phenology was registered according to [29]. The starting dates and duration of the most critical phenological stages observed during the first two growing seasons are reported in [9]. In Table S2, we again report all registered phenology and the observed data of season 2018–2019.

The soil moisture content was measured in the soil profile by using an FDR (Frequency Domain Reflectometer) or 'capacitance' sensor, the PR2 profile probe (DeltaT Devices Ltd., Cambridge, UK). Access tubes were placed at a depth of 1 m in the trials plots.

The leaf area index (LAI), the percentage of green canopy cover (CC), and the aboveground biomass (B), taken over a surface of 25 cm × 25 cm, were measured approximately every two weeks at each plot replicate. At the end of each crop cycle, corresponding to physiological maturity, the final aboveground biomass and grain yield (Y) were measured on a surface of 1 m^2 at the center of each plot. The aboveground biomass was determined by drying samples at 70 °C until they reached constant weight.

LAI was estimated by using the SunScan Canopy Analysis System (Delta-T Devices Ltd., Cambridge, UK). It measures both the incident photosynthetic active radiation (PAR) above canopy and the transmitted PAR through the canopy and calculates LAI from the Beer-Lambert extinction law by considering some major assumptions of both canopy and transmission of light (incident and diffuse). Three measurements were taken above and below the canopy in each plot.

The percentage of CC was estimated through zenithal digital RGB images taken above the canopy periodically in each plot (4 images/plot replicate). The images were processed using ImageJ software which detects the green vegetation and calculates the fraction of cover.

2.3. Satellite Data and Vegetation Indices

The high-resolution multispectral images from Sentinel-2A and 2B of the European Spatial Agency have been acquired during 2016–2017 and 2018–2019 growing seasons, respectively. The multi-spectral instrument (MSI) on board of Sentinel-2A/2B captures data at the spatial resolution of 10, 20 and 60 m over 13 spectral bands with a very high revisiting time of five days. The Sentinel-2 granules 36SYC Level-1C (processed at the top-of-atmosphere reflectance), which covers the target area in Lebanon, were acquired from the Copernicus Open Access Hub (https://scihub.copernicus.eu/).

The SNAP (Sentinels Application Platform) software version 6, developed by ESA as a Scientific Image Processing Toolbox, was used to process the Sentinel images and retrieve the vegetation indices required for the analysis. More specifically, the estimated vegetation indices in SNAP were the following: the Normalized Difference Vegetation index (NDVI), the Enhanced Vegetation Index (EVI), the Leaf Area Index (LAI), the fraction of Absorbed Photosynthetically Active Radiation (fAPAR) and the Fractional Vegetation Cover (FVC). In order to obtain a comparable time series, all indices were calculated based on atmospherically corrected Level-2A data.

NDVI was calculated using the processor of vegetation radiometric indices within the thematic land processing in SNAP by considering two Sentinel-2 spectral bands (B4-red and B8-infrared). The EVI was processed by using the Band Math in SNAP and applying the equation, as reported in [30]. The value range for EVI is −1 to 1, and it varies between 0.2 and 0.8 for healthy vegetation. EVI allows one to correct NDVI results for atmospheric influences and soil background signals, especially in areas of dense canopy. It is computed as:

$$\mathrm{EVI} = 2.5 * \frac{(\mathrm{NIR} - \mathrm{R})}{(1 + \mathrm{NIR} + 6\mathrm{R} - 7.5\mathrm{B})}$$

Here NIR is the near-infrared band 8, R is the red band 4, and B is the blue band 2.

LAI, f(APAR) and FVC were calculated using the biophysical processor in SNAP. The corresponding algorithms require eight Sentinel-2 spectral bands (B3–B7, B8a, B11 and B12) at 10 and 20 m (pixel size), which were all resampled to 10 m to derive the vegetation indices. Experimental studies have shown the accuracy of this approach for the estimation of LAI and other indices. For example, [31] reported that the SNAP biophysical processor would be applicable for versatile and rapid winter wheat parameter estimation. Finally, subsetting was also done to decrease both the image size and the processing time, and in order to cover only the investigated plots. Table S3 reports the Sentinel 2 acquisition dates used in this study in all years.

The estimated vegetation indices were correlated to the aboveground biomass obtained from field measurements through regression analysis to investigate the best-performing index. In addition, it was possible to compare LAI and FVC values estimated from remote sensing to those obtained from field data. This step was very important in understanding whether FVC would constitute a good vegetation index to be assimilated into AquaCrop, considering that coupling such an index derived from earth observation with a crop model would improve in the simulated crop growth and yield.

2.4. AquaCrop Model

2.4.1. Model Description, Calibration, and Validation

AquaCrop (AC) version 6.1 was used in this study. The model simulates crop growth in terms of biomass and yield in response to water and N inputs. As an indicator of the canopy size, AC uses the canopy cover (CC) equivalent to the fractional vegetation cover (FVC) estimated by Sentinel-2 imagery. The model was calibrated using the datasets of season 2016–2017 under full irrigation and rainfed cultivation. Then, it was validated with the data of seasons 2017–2018 and 2018–2019. The calibration was done through an iterative process using the observed phenological stages, measured crop growth variables, derived growing coefficients, and other parameters from the AquaCrop user manual.

The model validation is based on comparing observed and simulated data for all treatments using different datasets from those used for the model calibration. In particular, simulated and measured final biomass, harvestable yield, cumulative crop evapotranspiration, soil-water content, and canopy cover were compared for full irrigated and rainfed treatments of season 2017–2018 and season 2018–2019.

2.4.2. Coupling of AquaCrop and Sentinel Data

In this study, the methodology used to assess the coupling of AquaCrop with remote sensing as a tool to address irrigation management of wheat was based on the integration of Sentinel-2 crop-derived data with AquaCrop version 6.1. Therefore, FVC estimated by Sentinel-2 has been sequentially integrated into AquaCrop, by direct insertion, in place of the canopy cover (CC) simulated by the model. The sequential direct insertion is applied under the assumption that a continuous update of one crop model state based on remote observations can reduce the biases induced by the model simplifications of the processes and environmental conditions influencing the crop growth dynamics. This approach was also adopted by [15], by integrating Sentinel-2 Imagery data with AquaCrop for the dynamic assessment of tomato water requirements in Southern Italy.

2.4.3. Statistical Analysis

Some statistical indicators have been used to evaluate and compare the observed field data against those simulated by AquaCrop or derived from Sentinel 2 images. The root mean square error (RMSE), the coefficient of variation of the RMSE (CV (RMSE)), the index of agreement (d_IA), and the Nash–Sutcliffe coefficient (NSE), were applied as goodness-of-fit parameters to evaluate model performance, or derived vegetation indices against observed data.

The average difference between experimental data and simulation outputs is described by the root mean squared error (RMSE) as:

$$\mathrm{RMSE} = \left[\mathrm{N} \sum_{\mathrm{i}=1}^{\mathrm{N}} (\mathrm{P_i} - \mathrm{O_i})^2 \right]^{0.5}$$

where N is the number of pairs of observed/measured (O_i) and predicted/simulated (P_i) data.

The coefficient of variation of the RMSE (CV(RMSE)) was applied to normalize the RMSE to the mean of the observed/measured values ($\widetilde{O}$) as:

$$\mathrm{CV(RMSE)} = \frac{\mathrm{RMSE}}{\widetilde{\mathrm{O}}}$$

The index of agreement (d_{IA}), which represents the ratio between the mean square error and the "potential error", was calculated according to [32]:

$$\mathrm{d_{IA}} = 1 - \frac{\sum_{\mathrm{i}=1}^{\mathrm{n}} (\mathrm{O_i} + \mathrm{P_i})^2}{\sum_{\mathrm{i}=1}^{\mathrm{n}} \left(\left| \mathrm{P_i} - \widetilde{\mathrm{O}} \right| + \left| \mathrm{O_i} - \widetilde{\mathrm{O}} \right| \right)^2}$$

The d_{IA} is a descriptive parameter that varies between 0 and 1, with the value of 1.0 indicating excellent agreement.

Moreover, the Modelling Efficiency (NSE) was defined as:

$$\mathrm{NSE} = 1.0 - \frac{\sum_{\mathrm{i}=1}^{\mathrm{n}} (\mathrm{O_i} - \mathrm{P_i})^2}{\sum_{\mathrm{i}=1}^{\mathrm{n}} (\mathrm{O_i} - \widetilde{\mathrm{O}})^2}$$

This indicates the relative magnitude of the residual variance compared to the measured data variance [33,34]. According to [8,35], the validity of the model performance

was considered very good when the probability of fit showed an NSE = 0.9–1, good for NSE = 0.8–0.899, acceptable for NSE = 0.65–0.799, and unsatisfactory for NSE < 0.65.

3. Results and Discussion

3.1. Relationship between the Sentinel 2—Vegetation Indices and Field Data

Five vegetation indices were obtained from Sentinel-2 data during the growing seasons 2016–2017 and 2018–2019. Their trend is presented for different water treatments, going from rainfed until well-watered, in Figure 1. In general, the maximum NDVI values ranged between 0.54 (rainfed) and 0.84 (full irrigation) in the season 2016–2017 and between 0.87 (rainfed) and 0.91 (full irrigation) in 2018–2019. The higher values of NDVI for rainfed treatments in the last season are due to more significant precipitation explained by the wetter conditions that prevailed during that season. Similarly, EVI maximum values were between 0.51 and 0.63 in 2016–2017, while it reached a maximum value of 0.75 for all treatments in 2018–2019 regardless of their watering conditions. Maximum values of fAPAR ranged between 0.60 and 0.73 in 2016–2017 and between 0.80 and 0.83 in 2018–2019. Concerning maximum LAI and FVC, they were between 1.55 and 2.79, and 54% and 70%, respectively, for rainfed and irrigated treatments in 2016–2017, while they ranged between 3.73 and 3.88, and 76.7% and 78.8%, respectively in 2018–2019. Therefore, it was clear that most vegetation indices were higher in the 2018–2019 season than in 2016–2017 without a clear distinction between the values under rainfed or irrigated conditions. This behavior is closely linked to the higher precipitation amount and absence of water stress in 2018–2019 in respect to 2016–2017, as reported in the Section 2.1.

Regressions were fitted to relate biomass with S2 vegetation indices. Table 2 reports these relationships. The lowest and highest R^2 values (0.12 and 0.85) were found for EVI and FVC, respectively. In descending order of R^2, the indices were ranked FVC, LAI, fAPAR, NDVI and EVI. The use of EVI for monitoring long-term change of crops is debated. For example, [36] reported that this index presented some weakness compared to other vegetation indices; however [24] obtained satisfactory results for predicting yield and biomass production. Three R^2 values were above 0.70, one above 0.40, and one below 0.40. All simulated Sentinel-2 vegetation indices were fitted to power regression (Table 2). The results showed that biomass was associated with the vegetation indices. Particularly, FVC and LAI were highly correlated with biomass. Such findings agree with the study of [37], who found that LAI was highly correlated to maize biomass. The same was mentioned in the experiment implemented for the winter wheat crop by [21] where LAI showed a good correlation between Sentinel-2 estimates and the ground measurements. In addition, ref. [38] found that coupling FVC derived from satellite data with the AquaCrop model could provide the crop yield estimates in agreement with field data.

Table 2. Regressions of wheat biomass on Sentinel 2A vegetation indices.

Vegetation Index	Regression Models	R^2	RMSE (t ha^{-1})
NDVI	$y = 10.728x^{1.4315}$	0.68	2.26
EVI	$y = 3.8732x^{0.072}$	0.12	4.89
fAPAR	$y = 15.333x^{2.5657}$	0.71	1.09
LAI	$y = 2.7865x^{0.9011}$	0.78	1.90
FVC	$y = 0.0005x^{2.2673}$	0.85	1.34

y, biomass (t ha^{-1}); x, vegetation index.

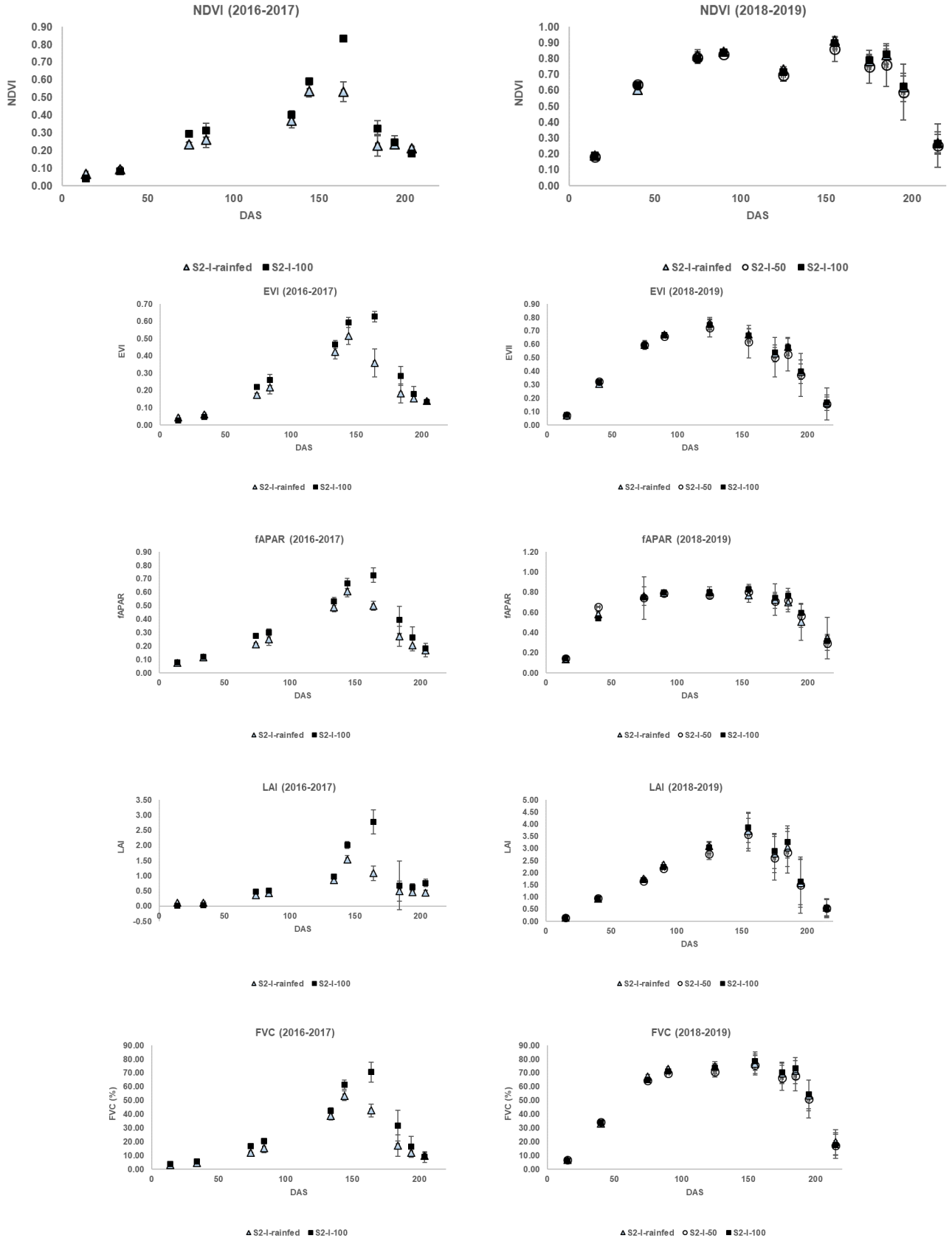

Figure 1. Trends of S2-derived vegetation indices for the growing seasons 2016–2017 and 2018–2019.

LAI and FVC derived indices from Sentinel 2 were also compared to the ground measurements, as reported in Figure 2. In general, there was a good fit between measured

data and those derived from S2 images. The regression between measured and S2 data is presented in Figure 3. The R^2 coefficient of 0.79 for canopy cover and 0.77 for LAI explains the good matching of measured and S2 derived data.

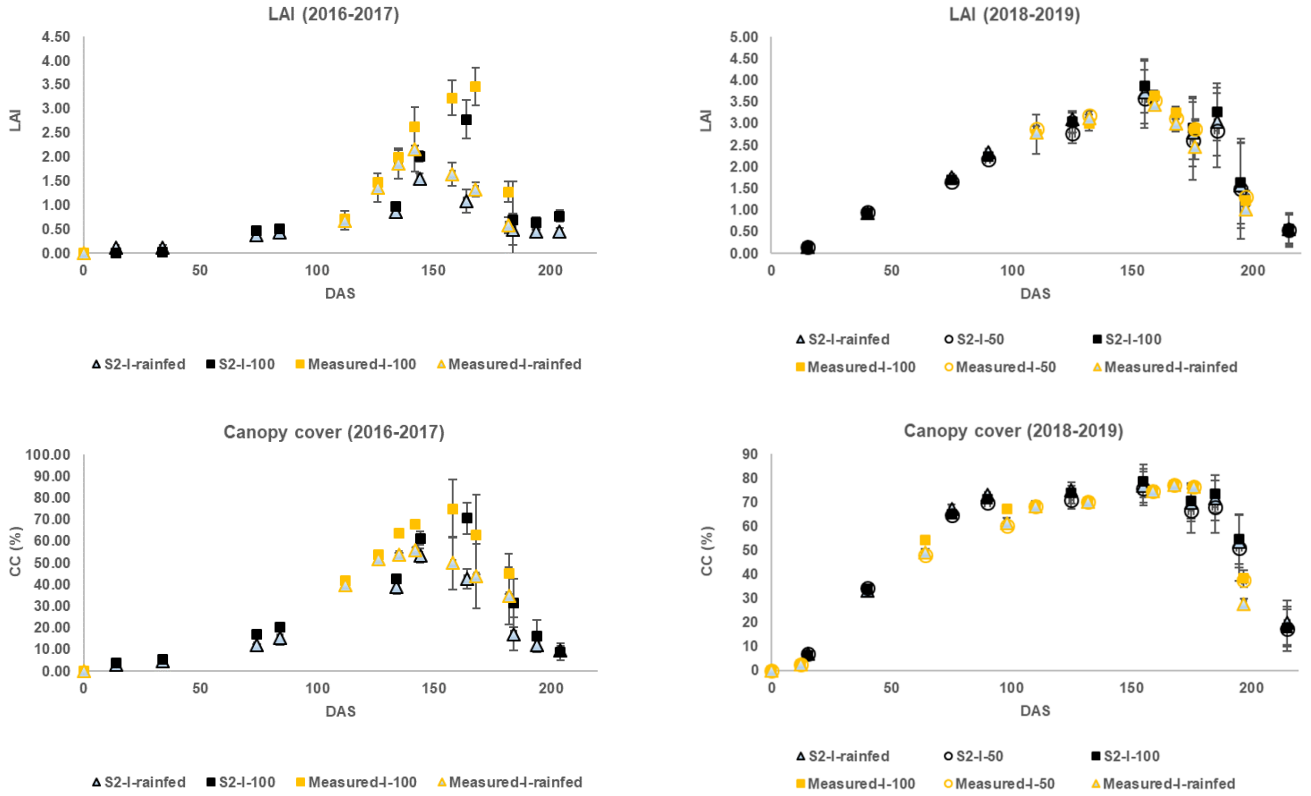

Figure 2. The seasonal trends of LAI and canopy cover (FVC) as compared to the ground measurements during the seasons 2016–2017 and 2018–2019.

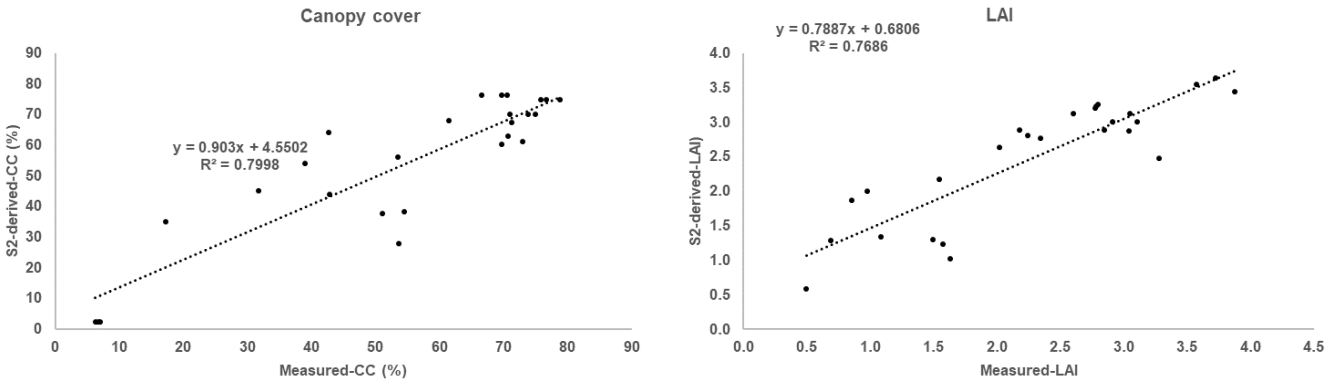

Figure 3. Regression between Sentinel 2 derived indices and measured LAI and CC.

3.2. Performance of AquaCrop Model to Simulate Winter Wheat Growth and Yield under Different Water Inputs

3.2.1. AquaCrop Calibration

The AquaCrop parameters for simulating the growth of winter wheat are presented in Table 3. These values were derived from calibration (c), direct field measurements (m), and estimations (e) from the dataset of season 2016–2017. Then, the values obtained by calibration were compared to those provided by the AquaCrop user manual as conservative parameters, which can be suitable to a wide range of conditions [39].

Table 3. Crop parameters used for wheat simulations by AquaCrop.

Parameter Description	Wheat Calibration	Method of Determination
Conservative parameters		
Base temperature (°C)	0	e **
Cut-off temperature (°C)	26	e
Canopy cover per seeding at 90% emergence (CC_0) (cm^2 $plant^{-1}$)	1.5	e
Canopy growth coefficient (CGC) (%/degree-day)	0.0061	c *
Crop coefficient for transpiration at CC = 100%	1.1	c
Canopy decline coefficient (CDC) at senescence (%/degree-day)	0.004	c
Biomass water productivity (WP), normalized for ETo before yield formation (g m^{-2})	16	e
Biomass water productivity, normalized for ETo during yield formation (% of WP)	100	e
Leaf growth threshold p-upper	0.2	c
Leaf growth threshold p-lower	0.55	c
Leaf growth stress coefficient curve shape	5	c
Stomatal conductance threshold p-upper	0.55	e
Stomata stress coefficient curve shape	0.5	c
Senescence stress coefficient p-upper	0.55	c
Senescence stress coefficient curve shape	2.5	c
Non-conservative parameters		
Time from sowing to emergence (GDD)	150	e
Maximum canopy cover (CCx) (%)	82	m ***
Time from sowing to start senescence (GDD)	1422	e
Time from sowing to maturity (GDD)	2451	e
Time from sowing to flowering (GDD)	1100	e
Maximum effective rooting depth, Zx (m)	1	m
Minimum effective rooting depth, Zn (m)	0.3	d ****
Reference harvest index, HI_o	45	m
GD range where crop transpiration is affected by cold stress (°C–day)	0–17.9	c

* c: calibration; ** e: estimation; *** m: measured; **** d: default.

Some of the conservative parameters were within the range proposed in the AquaCrop user manual (Raes et al., 2009). For example, the canopy growth coefficient (CGC) and the canopy decline coefficient (CDC) were set at 0.0061 and 0.004 percent per degree day, respectively, and these values are within the recommended range of 0.004–0.007 percent per degree day for the former and 0.004 percent per degree day for the latter. However, some other parameters, such as the water productivity (WP) for biomass, soil water depletion thresholds for inhibition of leaf growth, stomatal conductance, and the acceleration of canopy senescence, were different from those given in the AquaCrop user manual. The measured value of biomass water productivity used in the calibration for our wheat cultivar was 16 g m^{-2}, whereas the suggested value in the AquaCrop user manual is 15 g m^{-2}. Nevertheless, the calibrated value is still within the WP range of C_3 plants. The parameters that are cultivar specific or depending on management and environmental conditions were within the range mentioned in the manual. In general, the results of our calibration match the wheat parameters reported in the AquaCrop user manual [40]. In addition, most of the parameters were within the range obtained by [41], who conducted a global sensitivity analysis of the AquaCrop model for winter wheat under different water treatments in Beijing, China. Ref. [42] obtained similar ranges of values for the calibration of AquaCrop for winter wheat grown in Italy.

There was a significant relationship between data predicted by the model and those measured. The simulated yield varied from 1.92 to 3.70 t ha^{-1}, while the measured yield varied from 2.46 to 3.62 t ha^{-1} for rainfed and full irrigation treatments.

Results of observed and simulated values for calibration data sets (Table 4) show that for biomass, the most considerable differences were found for the treatments under rainfed conditions (−14.70%), whereas the percentage of deviation under full irrigation treatment was 0.04%. Also for yield, the largest differences were obtained for rainfed conditions (−21.83%). The reported percentage of deviation for sunflower yield reached 14.2% and 17.6% for irrigated and rainfed treatments, respectively [43]. For CC, the percentage of deviation, noted for I-100, was −0.24%, whereas the obtained percentage of deviation for I-rainfed was −2.62%.

Table 4. Simulation results for the calibration data set and deviation from measured values.

		Calibration Dataset		
Variables		**Measured**	**Simulated**	**% of Deviation**
Biomass (t ha^{-1})	I-100	10.7	10.7	0.04
	I-rainfed	8.4	7.2	−14.7
Yield (t ha^{-1})	I-100	3.6	3.7	2.1
	I-rainfed	2.5	2.0	−21.8
Canopy cover—CC (%)	I-100	82.0	81.8	−0.3
	I-rainfed	80.2	78.1	−2.6

The performance of the model, using the calibration dataset, was also evaluated for biomass, yield, CC and soil water depletion (SWD) through statistical indicators. The statistical indicators are reported in Table 5. The biomass's RMSE and the CV (RMSE) were respectively 0.62 and 0.12 t ha^{-1} under full irrigation conditions, and 1.34 and 0.36 t ha^{-1} under rainfed conditions. The index of agreement, dIA, and the modeling efficiency, NSE, were 0.99 and 0.99 for I-100 and 0.96 and 0.95 for I-rainfed. The yield RMSE and the CV (RMSE) were respectively 0.08 and 0.02 t ha^{-1} for I-100, and 0.54 and 0.22 t ha^{-1} for rainfed.

Table 5. Statistical indices derived for evaluating the performance of AquaCrop model in simulating biomass, yield, canopy cover, and soil water depletion for winter wheat (calibration dataset).

	Calibration Dataset							
	Biomass (t ha^{-1})		**Yield (t ha^{-1})**		**CC (%)**		**SWD (mm)**	
Statistical Indicators	**I-100**	**I-Rainfed**	**I-100**	**I-Rainfed**	**I-100**	**I-Rainfed**	**I-100**	**I-Rainfed**
RMSE	0.62	1.34	0.08	0.54	5.74	7.47	12.47	28.76
CV (RMSE)	0.12	0.36	0.02	0.22	0.13	0.11	0.12	0.58
d_{IA}	0.99	0.96	_	_	0.99	0.98	0.82	0.73
NSE	0.99	0.95	0.99	0.95	0.99	0.98	0.99	0.78

Simulated values of soil water depletion and canopy cover showed a good match with measured values, as demonstrated by the statistical indicators (Table 5). Going from full irrigation to rainfed conditions, RMSE, CV (RMSE), dIA, and NSE varied respectively from 12.47 to 28.76 mm, from 0.12 to 0.58 mm, from 0.82 to 0.73 and from 0.99 to 0.78 for soil water depletion simulations, whereas they varied respectively from 5.74 to 7.47%, from 0.13 to 0.11%, from 0.99 to 0.98 and from 0.99 to 0.98 for canopy cover simulations. The high RMSE values found for SWD question the robustness of the AquaCrop water balance module and its reliability to simulate water stress conditions for irrigation management planning purposes. Most studies on AquaCrop strongly link the model's performance under deficient irrigation to the duration and intensity of water stress, occurring during specific growth stages [11,41,43]. Consequently, the water balance module of the model should be examined more carefully under drought conditions and in harsh environments, as it is the case of Lebanon.

3.2.2. AquaCrop Validation

The parameters obtained in model calibration were used for validating the performance of AquaCrop by using independent data sets (2017–2018 and 2018–2019 growing seasons).

For season 2017–2018, there was a significant relationship between data predicted by the model and those measured: in fact, the simulated yield varied from 2.59 to 5.15 t ha^{-1}, while the measured yield varied from 3.08 to 5.63 t ha^{-1} for rainfed and full irrigation treatments, respectively. The simulation results and deviation from measured values are presented in Table 6.

Table 6. Simulation results for the validation data set and deviation from measured values.

		Validation Datasets					
		Season 2017–2018			Season 2018–2019		
Variables		**Measured**	**Simulated**	**% of Deviation**	**Measured**	**Simulated**	**% of Deviation**
Biomass (t ha^{-1})	I-100	10.8	10.4	−3.9	15.0	15.6	3.9
	I-50	_	_	_	14.2	15.4	8.5
	I-rainfed	6.8	7.7	13.8	12.2	15.0	23.3
Yield (t ha^{-1})	I-100	5.6	5.1	−9.3	5.3	5.4	1.7
	I-50	_	_	_	4.8	5.2	9.7
	I-rainfed	3.1	2.6	−18.9	4.3	5.0	16.1
Canopy cover (%)	I-100	75	81.7	8.9	77.3	81.8	5.8
	I-50	_	_	_	77.0	81.8	6.2
	I-rainfed	69	80	15.9	76.9	81.8	6.4

In season 2018–2019, although the growing season was characterized by high rainfall, a total precipitation amount of 825 mm, AquaCrop predicted one irrigation event on 15 May 2019 during the grain filling stage (milk stage). The total net irrigation amount, as advised by AquaCrop, was 72.6 mm for the I-100 treatment and 36.3 mm for I-50. Such environmental conditions prevented obtaining substantial differentiation between treatments for both biomass and yields. The largest differences between observed and simulated biomass values were observed for the treatments under rainfed conditions (23.31%), while the percentage of deviation under full irrigation treatment was 3.86%. The most significant differences between observed and simulated yield values were also reported for rainfed conditions (16.11%). For CC, the percentage of deviation was 5.78% for I-100, whereas it was 6.39% for I-rainfed.

The calculated values of statistical indices are reported in Table 7. In the 2017–2018 season, the RMSE and the CV (RMSE) of biomass were respectively 0.67 and 0.13 t ha^{-1} under full irrigation, 0.92 and 0.26 t ha^{-1} under rainfed conditions. The dIA and The NSE were 0.98 and 0.99 for irrigated, 0.98 and 0.96 for rainfed conditions. The yield RMSE and CV (RMSE) were respectively 1.48 and 0.26 t ha^{-1} for I-100, and 0.70, 0.23 t ha^{-1} for I-rainfed. The NSE were respectively 0.93 and 0.95 confirming the goodness of fit between measured and simulated values.

Table 7. Statistical indices derived for evaluating the performance of the AquaCrop model in simulating biomass, yield, canopy cover, and soil water depletion for winter wheat (2017–2018 and 2018–2019 datasets).

						Season 2017–2018						
	Biomass (t ha^{-1})			**Yield (t ha^{-1})**			**CC (%)**			**SWD (mm)**		
Statistical Indicators	**I-100**	**I-50**	**I-Rainfed**	**I-100**	**I-50**	**I-Rainfed**	**I-100**	**I-50**	**I-Rainfed**	**I-100**	**I-50**	**I-Rainfed**
RMSE	0.67	_	0.92	1.48	_	0.7	11.11	_	21.48	21.93	_	29.34
CV (RMSE)	0.13	_	0.26	0.26	_	0.23	0.21	_	0.51	0.16	_	0.32
d_{IA}	0.98	_	0.98	_	_	_	0.95	_	0.77	0.75	_	0.72
NSE	0.99	_	0.96	0.93	_	0.95	0.98	_	0.86	0.98	_	0.9
						Season 2018–2019						
RMSE	1.32	1.36	1.6	0.09	0.46	0.69	6.99	7.16	9.49	10.97	14.33	17.25
CV (RMSE)	0.21	0.22	0.27	0.02	0.1	0.16	0.14	0.14	0.19	0.33	0.4	0.43
d_{IA}	0.99	0.99	0.98	_	_	_	0.99	0.99	0.98	0.87	0.78	0.83
NSE	0.98	0.98	0.97	0.99	0.99	0.97	0.99	0.99	0.97	0.96	0.94	0.93

The RMSE, CV (RMSE), dIA and NSE varied respectively from 21.93 to 29.34 mm, from 0.16 to 0.32 mm, from 0.75 to 0.72, and from 0.98 to 0.90 for soil water content simulations, whereas they varied respectively from 11.11% to 21.48%, from 0.21% to 0.51%, from 0.95 % to 0.77%, and from 0.98% to 0.86% for canopy cover simulations.

In the 2018–2019 season, the RMSE and the CV (RMSE) of biomass were 1.32 and 0.21 t ha^{-1} under full irrigation, 1.36 and 0.22 t ha^{-1} under deficit irrigation, 1.60 and

0.27 t ha^{-1} for rainfed conditions. The NSE was respectively 0.98, 0.98 and 0.97 for irrigated, deficit, and rainfed conditions, whereas the dIA were 0.99, 0.99 and 0.98, respectively. The yield RMSE and the CV (RMSE) were respectively 0.09 and 0.02 t ha^{-1} for I-100, 0.46 and 0.10 t ha^{-1} for deficit irrigation, 0.69 and 0.16 t ha^{-1} for I-rainfed. The NSE were 0.99, 0.99 and 0.97, confirming the goodness of fit between measured and simulated values.

The RMSE and the CV (RMSE) varied respectively from 10.97 to 17.25 mm and from 0.33 to 0.43 mm for soil water content simulations, whereas they varied respectively from 6.99% to 9.49%, from 0.14% to 0.19% for canopy cover simulations. dIA and NSE varied from 0.83 to 0.87 and from 0.93 to 0.96 for soil water content simulations, and from 0.98 to 0.99 and from 0.97 to 0.99 for canopy cover simulations.

3.3. Results of S2-Derived CC Insertion in AquaCrop

After deriving the CC from S2 images of seasons 2016–2017 and 2018–2019, the maximum values, as obtained for the different water conditions, were inserted into the AquaCrop model. The simulations were run for two growing seasons: 2016–2017 and 2018–2019. Simulated results for biomass, yield, and canopy cover (CC) were again evaluated with respect to the ground measurements, as presented in Table S4. In the 2016–2017 season, the largest difference between observed and simulated values for biomass was shown for the treatment under rainfed conditions (−9.25%), whereas the percentage of deviation under irrigated treatment was −1.58%. The largest difference between observed and simulated yield values was also reported for rainfed conditions (−17.07%). The percentage of deviation, noted for CC of I-100 treatment was −1.34%, whereas the obtained percentage of deviation for I-rainfed was −5.61%. In the 2018–2019 season, the largest difference between observed and simulated values for biomass was reported for the treatment under rainfed condition (18.56%), whereas the percentage of deviation under full-irrigation treatment was 1.32% and 3.45% for deficit irrigation. The largest difference between observed and simulated yield values was also reported for rainfed conditions (12.17%), whereas the percentage of deviation under full irrigation treatment was −0.76% and 4.85% for deficit irrigation. For CC, the percentage of deviation was 1.9% and −0.8% for I-100 and I-50, respectively, whereas the obtained percentage of deviation for I-rainfed was −1.29%. The calculated values of statistical indices are reported in Table 8.

Table 8. Statistical indices derived for evaluating the performance of AquaCrop model in simulating biomass, yield, canopy cover, and soil water depletion for winter wheat (2016–2017 and 2018–2019 datasets) after S2-CC assimilation.

	2016–2017 Dataset											
	Biomass (t ha^{-1})			**Yield (t ha^{-1})**			**CC (%)**			**SWD (mm)**		
Statistical Indicators	**I-100**	**I-50**	**I-Rainfed**	**I-100**	**I-50**	**I-Rainfed**	**I-100**	**I-50**	**I-Rainfed**	**I-100**	**I-50**	**I-Rainfed**
RMSE	1.06	_	0.48	0.05	_	0.34	4.45	_	5.65	24.45	_	21.96
CV (RMSE)	0.2	_	0.14	0.3	_	0.24	0.09	_	0.13	0.27	_	0.16
d_{IA}	0.98	_	0.99	_	_	_	0.99	_	0.98	0.82	_	0.84
NSE	0.98	_	0.99	0.91	_	0.96	1	_	0.99	0.93	_	0.98
	2018–2019 Dataset											
RMSE	1.15	1	1.26	0.04	0.23	0.42	5.28	4.42	7.17	10.86	14.43	17.54
CV (RMSE)	0.18	0.16	0.21	0.01	0.05	0.12	0.11	0.09	0.15	0.33	0.4	0.44
d_{IA}	0.99	0.99	0.99	_	_	_	0.99	0.99	0.98	0.87	0.77	0.74
NSE	0.99	0.99	0.98	1	1	0.99	0.99	0.99	0.99	0.96	0.94	0.93

Figure 4 shows a comparison between the percentage of deviation of simulations in respect to measured data for biomass, yield, and CC, with and without S2-CC integration into AquaCrop. The figure clearly shows that, in season 2018–2019, after assimilating the S2-CC into AquaCrop, the percentage of deviation between simulated and measured data is decreased, confirming that remote sensing data would offer a great potential for crop yield prediction and irrigation monitoring.

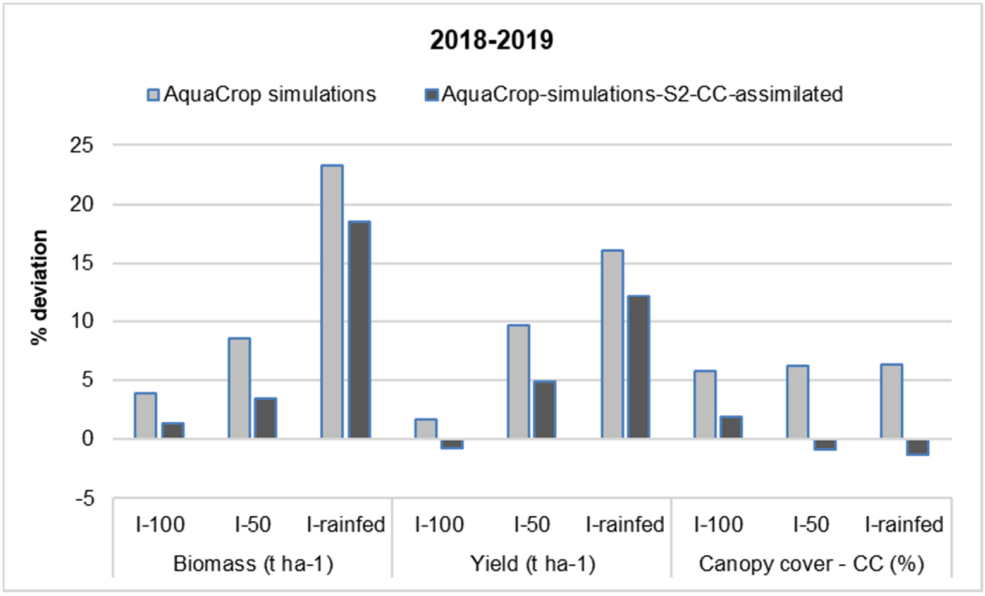

Figure 4. Percentage of deviation between simulated and measured variables before and after S2-CC assimilation into AquaCrop for 2018–2019.

Overall, the insertion of remote sensing data into crop models would present an opportunity for crop yield forecasting. In fact, [21] obtained similar findings after integrating LAI in the EPIC model providing an improvement in wheat yield estimation and indicated that the combination framework must be tested under different environmental conditions before being applied on a larger scale. Ref. [22] presented an approach for assimilating FVC for wheat grown in Belgium into AquaCrop, resulting in a RMSE for yield of 0.8 t ha^{-1}. In the present study, the RMSE was much lower for wheat grown in Lebanon, i.e., 0.34 to 0.42 t ha^{-1} under rainfed conditions and 0.04 to 0.05 t ha^{-1} under irrigated conditions. Coupling AquaCrop and satellite-derived Fractional Vegetation Cover also offered a good potential for maize grown prediction in Belgium under rainfed conditions, with biomass RMSE of 0.7 t ha^{-1} [11].

It is important to establish a robust integration approach of remote sensing derived data into crop models to increase the estimation accuracy of crop biomass and yield. This issue was raised by different authors, among them [37], who reported that the estimation accuracy for maize yield in China was improved when using a double-variable data assimilation approach (by assimilating FVC and biomass) into AquaCrop (RMSE for biomass dropped from 2.51 to 1.44 tons ha^{-1}) as compared to use of a single-variable data assimilation approach (only FVC). In our study, the simulation accuracy of AquaCrop after integrating the satellite-derived CC was improved by 40% for yield prediction. Such results agree with the findings of [23], who reported a 26% to 36% improvement in wheat yield simulation accuracy after combining AquaCrop with derived parameters from remote sensing data. Similarly, [44] found that AquaCrop's capability to simulate maize yield was improved by 12% after integrating CC derived from remotely sensed NDVI. A robust assimilation approach would also improve the irrigation water requirement predictions [15], as investigated in Southern Italy on the tomato crop. Ref. [23] also demonstrated that maize grown in China was improved by 20% in regional crop water consumption and by 26–36% in regional yield when coupling AquaCrop and remote sensing. Recent studies generated more evidence on the development of near-real-time irrigation scheduling approaches by integrating of in situ soil moisture data and crop evapotranspiration data derived from satellite images. Such approach was tested by [45] on a tomato crop grown in Canada.

Finally, coupling AquaCrop and remote sensing could be an effective and promising method of crop model upscaling once achieving a robust integration framework.

4. Conclusions

The potential of the AquaCrop model to simulate biomass and yield of winter wheat in a semi-arid Mediterranean region was successfully assessed. Moreover, the gathered experiences support the operational use of spectral inputs for irrigation scheduling and simulation of crop development and growth in the Mediterranean. In this study, plenty of new opportunities are promoted by the use of available satellite FVC data at the field scale. Combined with crop growth models, monitoring vast regions of agricultural fields is possible, and the performance of existing yield forecasting models is improved. More investigation and additional data are needed to establish a robust integration network under different environmental conditions and water management practices.

Supplementary Materials: The following are available online at https://www.mdpi.com/article/10.3390/agronomy11112265/s1. Figure S1: The location of the study area and the field trials, Table S1: Soil characteristics of the field during the three growing seasons, Table S2: Experimental details and dates of the main phenological stages for durum wheat during the growing seasons 2016–2017, 2017–2018 and 2018–2019. In brackets the days after sowing (DAS) are reported, Table S3: List of Sentinel 2 acquisition dates, Table S4: Simulation results for the seasons 2016–2017 and 2018–2019 and deviation from measured values after assimilating S2-CC.

Author Contributions: Conceptualization, M.T.A.S. and M.T.; methodology, M.T.A.S.; software, M.T.A.S. and R.E.A.; field work, I.J.; S.F., S.S. and R.E.A.; formal analysis, M.T.A.S., R.A. and M.T.; writing—original draft preparation, M.T.A.S.; writing—review and editing, M.T.A.S. and R.A.; supervision, R.A. and M.T. All authors have read and agreed to the published version of the manuscript.

Funding: This research was carried out under the Master of Science Program on "Sustainable water and land management in Mediterranean agriculture" funded by CIHEAM—Mediterranean Institute of Bari.

Institutional Review Board Statement: Not applicable.

Informed Consent Statement: Not applicable.

Data Availability Statement: The datasets and the R codes used in this study are available from the authors upon reasonable request.

Conflicts of Interest: The authors declare no conflict of interest.

References

1. Hubert, B.; Rosegrant, M.; Van Boekel, M.A.; Ortiz, R. The future of food: Scenarios for 2050. *Crop. Sci.* **2010**, *50*, 33–50. [CrossRef]
2. Keating, B.A.; Carberry, P.S.; Bindraban, P.S.; Asseng, S.; Meinke, H.; Dixon, J. Eco-efficient agriculture: Concepts, challenges, and opportunities. *Crop Sci.* **2010**, *50*, 109–119. [CrossRef]
3. FAO. Faostat-Trade/Crops and Livestock Products. 2016. Available online: http://faostat3.fao.org/browse/T/TP/E (accessed on 5 May 2016).
4. Nabavi-Pelesaraei, A.; Hosseinzadeh-Bandbafha, H.; Qasemi-Kordkheili, P.; Kouchaki-Penchah, H.; Riahi-Dorcheh, F. Applying optimization techniques to improve of energy efficiency and GHG (greenhouse gas) emissions of wheat production. *Energy* **2016**, *103*, 672–678. [CrossRef]
5. FAOSTAT. FAOSTAT Agriculture Data. 2017. Available online: http://www.fao.org/faostat/en/#data/QC (accessed on 20 July 2019).
6. Mondal, S.; Singh, R.P.; Mason, E.R.; Huerta-Espino, J.; Autrique, E.; Joshi, A.K. Grain yield, adaptation and progress in breeding for early-maturing and heat-tolerant wheat lines in South Asia. *Field Crop. Res.* **2016**, *192*, 78–85. [CrossRef] [PubMed]
7. MoA/FAO. *Agricultural Census 2010*; FAO: Rome, Italy, 2010.
8. Abi Saab, M.T.; Jomaa, I.; Skaf, S.; Fahed, S.; Todorovic, M. Assessment of a Smartphone Application for Real-Time Irrigation Scheduling in Mediterranean Environments. *Water* **2019**, *11*, 252. [CrossRef]
9. Abi Saab, M.T.; Sellami, M.H.; Giorio, P.; Basile, A.; Bonfante, A.; Rouphael, Y.; Fahed, S.; Jomaa, I.; Stephan, C.; Kabalan, R.; et al. Assessing the Potential of Cereal Production Systems to Adapt to Contrasting Weather Conditions in the Mediterranean Region. *Agronomy* **2019**, *9*, 393. [CrossRef]
10. Han, C.; Zhang, B.; Chen, H.; Wei, Z.; Liu, Y. Spatially distributed crop model based on remote sensing. *Agric. Water Manag.* **2019**, *218*, 165–173. [CrossRef]

11. Sallah, A.H.M.; Tychon, B.; Piccard, I.; Gobin, A.; Hoolst, R.V.; Djaby, B.; Wellens, J. Batch-processing of AquaCrop plug-in for rainfed maize using satellite derived Fractional Vegetation Cover data. *Agric. Water Manag.* **2019**, *217*, 346–355. [CrossRef]
12. Dente, L.; Satalino, G.; Mattia, F.; Rinaldi, M. Assimilation of leaf area index derived from ASAR and MERIS data into CERES-Wheat model to map wheat yield. *Remote Sens. Environ.* **2008**, *112*, 1395–1407. [CrossRef]
13. De Wit, A.D.; Van Diepen, C.A. Crop model data assimilation with the Ensemble Kalman filter for improving regional crop yield forecasts. *Agric. For. Meteorol.* **2007**, *146*, 38–56. [CrossRef]
14. Fang, H.; Liang, S.; Hoogenboom, G. Integration of MODIS LAI and vegetation index products with the CSM–CERES–Maize model for corn yield estimation. *Int. J. Remote Sens.* **2011**, *32*, 1039–1065. [CrossRef]
15. Dalla Marta, A.; Chirico, G.B.; Falanga Bolognesi, S.; Mancini, M.; D'Urso, G.; Orlandini, S.; De Michele, C.; Altobelli, F. Integrating Sentinel-2 Imagery with AquaCrop for Dynamic Assessment of Tomato Water Requirements in Southern Italy. *Agronomy* **2019**, *9*, 404. [CrossRef]
16. De Wit, A.; Duveiller, G.; Defourny, P. Estimating regional winter wheat yield with WOFOST through the assimilation of green area index retrieved from MODIS observations. *Agric. For. Meteorol.* **2012**, *164*, 39–52. [CrossRef]
17. Ma, G.; Huang, J.; Wu, W.; Fan, J.; Zou, J.; Wu, S. Assimilation of MODIS-LAI into the WOFOST model for forecasting regional winter wheat yield. *Math. Comput. Model.* **2013**, *58*, 634–643. [CrossRef]
18. Fabian, L.; Chandrashekhar, M.B.; Fliemann, E.; Lamers, J.P.A.; Conrad, C. Assessing gaps in irrigated agricultural productivity through satellite earth observations—A case study of the Fergana Valley, Central Asia. *Int. J. Appl. Earth Obs. Geoinf.* **2017**, *59*, 118–134.
19. Yi, C.; Zhao, Z.; Fulu, T. Improving regional winter wheat yield estimation through assimilation of phenology and leaf area index from remote sensing data. *Eur. J. Agron.* **2018**, *101*, 163–173.
20. Guerif, M.; Duke, C.L. Adjustment procedures of a crop model to the site specific characteristics of soil and crop using remote sensing data assimilation. *Agric. Ecosyst. Environ.* **2000**, *81*, 57–69. [CrossRef]
21. Novelli, F.; Spiegel, H.; Sandén, T.; Vuolo, F. Assimilation of sentinel-2 leaf area index data into a physically-based crop growth model for yield estimation. *Agronomy* **2019**, *9*, 255. [CrossRef]
22. Wellens, J.; Sallah, A.H.; Tychon, B. Assessment of AquaCrop for winter wheat using satellite derived fCover data. In Proceedings of the 9th International Workshop on the Analysis of Multitemporal Remote Sensing Images (MultiTemp), Brugge, Belgium, 27–29 June 2017; pp. 1–3.
23. Han, C.; Zhang, B.; Chen, H.; Liu, Y.; Wei, Z. Novel approach of upscaling the FAO AquaCrop model into regional scale by using distributed crop parameters derived from remote sensing data. *Agric. Water Manag.* **2020**, *240*, 106288. [CrossRef]
24. Jin, X.; Li, Z.; Feng, H.; Ren, Z.; Li, S. Estimation of maize yield by assimilating biomass and canopy cover derived from hyperspectral data into the AquaCrop model. *Agric. Water Manag.* **2020**, *227*, 105846. [CrossRef]
25. Allen, R.G.; Pereira, L.S.; Raes, D.; Smith, M. *Guidelines for Computing Crop Water Requirements-FAO Irrigation and Drainage Paper 56*; FAO-Food and Agriculture Organisation of the United Nations: Rome, Italy, 1998. Available online: http://www.fao.org/docrep (accessed on 20 July 2019).
26. FAO. *Guidelines for Soil Description*, 4th ed.; Food and Agriculture Organization of the United Nations: Rome, Italy, 2006. Available online: http://www.fao.org/publications/card/en/c/903943c7-f56a-521a-8d32-459e7e0cdae9/ (accessed on 20 July 2019).
27. IUSS Working Group, W.R.B. *World Reference Base for Soil Resources 2014. International Soil Classification System for Naming Soils and Creating Legends for Soil Maps*; World Soil Resources Reports 106; Sales and Marketing Group: Rome Italy, 2014. [CrossRef]
28. Saxton, K.E.; Rawls, W.J. Soil water characteristic estimates by texture and organic matter for hydrologic solutions. *Soil Sci. Soc. Am. J.* **2006**, *70*, 1569–1578. [CrossRef]
29. Zadoks, J.C.; Chang, T.T.; Konzak, C.F. A decimal code for the growth stages of cereals. *Weed Res.* **1974**, *14*, 415–421. [CrossRef]
30. Huete, A.R.; Liu, H.Q.; Batchily, K.V.; Van Leeuwen, W.J.D.A. A comparison of vegetation indices over a global set of TM images for EOS-MODIS. *Remote Sens. Environ.* **1997**, *59*, 440–451. [CrossRef]
31. Xie, Q.; Dash, J.; Huete, A.; Jiang, A.; Yin, G.; Ding, Y.; Peng, D.; Hall, C.C.; Brown, L.; Shi, Y.; et al. Retrieval of crop biophysical parameters from Sentinel-2 remote sensing imagery. *Int. J. Appl. Earth Obs. Geoinf.* **2019**, *80*, 187–195. [CrossRef]
32. Willmott, C.J. Some comments on the evaluation of model performance. *Bull. Am. Meteorol. Soc.* **1982**, *63*, 1309–1313. [CrossRef]
33. Nash, J.E.; Sutcliffe, J.V. River flow forecasting through conceptual models part I—A discussion of principles. *J. Hydrol.* **1970**, *10*, 282–290. [CrossRef]
34. Moriasi, D.N.; Arnold, J.G.; Van Liew, M.W.; Bingner, R.L.; Harmel, R.D.; Veith, T.L. Model evaluation guidelines for systematic quantification of accuracy in watershed simulations. *Trans. ASABE* **2007**, *50*, 885–900. [CrossRef]
35. Mbabazi, D.; Migliaccio, K.W.; Crane, J.H.; Fraisse, C.; Zotarelli, L.; Morgan, K.T.; Kiggundu, N. An irrigation schedule testing model for optimization of the Smartirrigation avocado app. *Agric. Water Manag.* **2017**, *179*, 390–400. [CrossRef]
36. Xie, Q.; Huang, W.; Dash, J.; Song, X.; Huang, L.; Zhao, J.; Wang, R. Evaluating the potential of vegetation indices for winter wheat LAI estimation under different fertilization and water conditions. *Adv. Space Res.* **2015**, *56*, 2365–2373. [CrossRef]
37. Jin, X.; Li, Z.; Feng, H.; Ren, Z.; Li, S. Deep neural network algorithm for estimating maize biomass based on simulated Sentinel 2A vegetation indices and leaf area index. *Crop J.* **2020**, *8*, 87–97. [CrossRef]
38. Silvestro, P.; Pignatti, S.; Pascucci, S.; Yang, H.; Li, Z.; Yang, G.; Huang, W.; Casa, R. Estimating wheat yield in China at the field and district scale from the assimilation of satellite data into the Aquacrop and simple algorithm for yield (SAFY) models. *Remote Sens.* **2017**, *9*, 509. [CrossRef]

39. Hsiao, T.C.; Heng, L.; Steduto, P.; Rojas-Lara, B.; Raes, D.; Fereres, E. AquaCrop—The FAO crop model to simulate yield response to water: III. Parameterization and testing for maize. *Agron. J.* **2009**, *101*, 448–459. [CrossRef]
40. Raes, D.; Steduto, P.; Hsiao, T.C.; Fereres, E. AquaCrop—The FAO crop model to simulate yield response to water: II. Main algorithms and software description. *Agron. J.* **2009**, *101*, 438–447. [CrossRef]
41. Xing, H.; Xu, X.; Li, Z.; Chen, Y.; Feng, H.; Yang, G.; Chen, Z. Global sensitivity analysis of the AquaCrop model for winter wheat under different water treatments based on the extended Fourier amplitude sensitivity test. *J. Integr. Agric.* **2017**, *16*, 2444–2458. [CrossRef]
42. Trombetta, A.; Iacobellis, V.; Tarantino, E.; Gentile, F. Calibration of the AquaCrop model for winter wheat using MODIS LAI images. *Agric. Water Manag.* **2016**, *164*, 304–316. [CrossRef]
43. Stricevic, R.; Cosic, M.; Djurovic, N.; Pejic, B.; Maksimovic, L. Assessment of the FAO AquaCrop model in the simulation of rainfed and supplementally irrigated maize, sugar beet and sunflower. *Agric. Water Manag.* **2011**, *98*, 1615–1621. [CrossRef]
44. Tsakmakis, I.D.; Gikas, G.D.; Sylaios, G.K. Integration of Sentinel-derived NDVI to reduce uncertainties in the operational field monitoring of maize. *Agric. Water Manag.* **2021**, *255*, 106998. [CrossRef]
45. Ihuoma, S.O.; Madramootoo, C.A.; Kalacska, M. Integration of satellite imagery and in situ soil moisture data for estimating irrigation water requirements. *Int. J. Appl. Earth Obs. Geoinf.* **2021**, *102*, 102396. [CrossRef]